

# NMR relaxation rate and static spin susceptibility in graphene

Tianxing Ma, Balázs Dóra

Max-Planck-Institut für Physik Komplexer Systeme, Nöthnitzer Str. 38, 01187 Dresden, Germany

(Dated: February 17, 2008)

The NMR relaxation rate and the static spin susceptibility in graphene are studied within a tight-binding description. At half filling, the NMR relaxation rate follows a power law as  $T^2$  on the particle-hole symmetric side, while with a finite chemical potential  $\mu$  and next-nearest neighbor  $t'$ , the  $(\mu + 3t')^2$  terms dominate at low excess charge  $\delta$ . The static spin susceptibility is linearly dependent on temperature  $T$  at half filling when  $t' = 0$ , while with a finite  $\mu$  and  $t'$ , it should be dominated by  $(\mu + 3t')$  terms in low energy regime. These unusual phenomena are direct results of the low energy excitations of graphene, which behave as massless Dirac fermions. Furthermore, when  $\delta$  is high enough, there is a pronounced crossover which divides the temperature dependence of the NMR relaxation rate and the static spin susceptibility into two temperature regimes: the NMR relaxation rate and the static spin susceptibility increase dramatically as temperature increases in the low temperature regime, and after the crossover, both decrease as temperature increases at high temperatures. This crossover is due to the well-known logarithmic Van Hove singularity in the density of states, and its position dependence of temperature is sensitive to  $\delta$ .

PACS numbers: 81.05.Uw, 71.10.-w, 72.15.-v

## I. INTRODUCTION

Graphene, the latest carbon allotrope to be discovered<sup>1</sup>, is made out of carbon atoms organized into a honeycomb lattice. The characteristics of the honeycomb lattice make graphene a half filled system with a density of states (DOS) that vanishes linearly at the neutrality point, and an effective, low energy quasi-particle spectrum characterized by a dispersion which is linear in momentum close to the Fermi energy<sup>2</sup>. These two features underlie the unconventional electronic properties of this material, whose low energy excitations behave as massless Dirac fermions<sup>3,4</sup>.

There have been intensive theoretical and experimental studies on graphene to this date, for instance, half integer and unconventional quantum Hall effect<sup>5,6,7,8</sup>, quantum minimum conductivity<sup>5,9,10</sup>, bipolar supercurrent<sup>11</sup>, ferromagnetism<sup>12</sup>, optical conductivity<sup>13</sup> and the possibility of superconductivity<sup>14</sup>. On the other hand, the most interesting and promising properties from the technological point of view are its great crystalline quality, high mobility and resilience to very high current densities<sup>4</sup>, the ability to tune the carrier density through a gate voltage<sup>1</sup>, as well as the fact that graphene exhibits both spin and valley degrees of freedom which might be harnessed in envisaged spintronics<sup>15,16,17</sup>. For a review of other remarkable properties of such systems as well as a discussion of possible technological applications, the reader is referred to Ref.<sup>4,18</sup>. Graphene is poised to become a new paradigm in solid state physics and materials science.

Nuclear magnetic resonance (NMR) is usually an excellent technique for probing the electronic properties of materials as it is sensitive to the DOS near the Fermi edge, and this method allows one to study static magnetic correlations and low-energy spin excitations. For a material with a Fermi liquid state, the temperature de-

pendent spin-lattice relaxation time  $T_1$  follows the well-known Korringa relation where  $1/T_1$  varies linearly with temperature<sup>19</sup>. As one of the most powerful methods for investigating mechanisms of superconductivity of the many exotic types of superconductors being discovered today, it has turned out that the explanation for the peak in the NMR relaxation rate just in superconducting state was that the DOS peaked dramatically at the edge of a energy gap<sup>19,20</sup>. Recent NMR experiments by Singer *et al.* showed a deviation from Fermi liquid behavior in carbon nanotubes with an energy gap evident at low temperatures<sup>21</sup>. In the framework of the Tomonaga-Luttinger liquid, the low temperature properties are governed by a gapped relaxation due to a spin gap, which crosses over smoothly to the Luttinger liquid behavior with increasing temperature<sup>22</sup>.

In spite of being few atoms thick, the system of graphene was found to be stable and ready for exploration<sup>4</sup>, and, it is believed that NMR should provide cornucopian and significant information on the electronic properties of graphene<sup>19</sup>. In the present paper, we study the NMR relaxation rate and the static spin susceptibility of graphene within a tight-binding description. At half filling, the NMR relaxation rate follows a power law as  $T^2$  on the particle-hole symmetric side, while away from half filling and with a finite next-nearest neighbor  $t'$ , the  $(\mu + 3t')^2$  terms dominate at low excess charge  $\delta$ . The static spin susceptibility is linearly dependent on temperature  $T$  at half filling when  $t' = 0$ , while with a finite  $\mu$  and  $t'$ , it should be dominated by  $(\mu + 3t')$  terms in low energy regime. These unusual phenomena are direct results of the low energy excitations of graphene, which behave as massless Dirac fermions. Furthermore, when  $\delta$  is high enough, there is a pronounced crossover which divides the temperature dependence of the NMR relaxation rate and the static spin susceptibility into two temperature regimes: the NMR relaxation rate and the

static spin susceptibility increase dramatically as temperature increases in the low temperature regime, and after the crossover, both decrease as temperature increases at high temperatures. This crossover is due to the well-known logarithmic Van Hove singularity in the DOS, and its position dependence of temperature is sensitive to  $\delta$ .

The rest of the paper is organized as follows. The theoretical framework is introduced in section II. Our numerical result and discussion are shown in section III, and the paper is concluded with a summary in section IV.

## II. THEORETICAL FRAMEWORK

Graphene is a two dimensional crystal of carbon atoms with a honeycomb lattice, which can be described in terms of two interpenetrating triangular sublattices, A and B, and then the electronic structure of graphene can be captured within a tight-binding description<sup>18,23,24,25</sup>

$$H = -t \sum_{i\eta\sigma} (a_{i\sigma}^\dagger b_{i+\eta\sigma}) + t' \sum_{i\gamma\sigma} (a_{i\sigma}^\dagger a_{i+\gamma\sigma} + b_{i\sigma}^\dagger b_{i+\gamma\sigma}) + \text{h.c.} \\ + \mu \sum_{i\sigma} (a_{i\sigma}^\dagger a_{i\sigma} + b_{i\sigma}^\dagger b_{i\sigma}), \quad (1)$$

where  $a_{i,\sigma}$  ( $a_{i,\sigma}^\dagger$ ) annihilates (creates) electrons at the site  $\mathbf{R}_i$  with spin  $\sigma$  ( $\sigma = \uparrow, \downarrow$ ) on sublattice A, and  $b_{i,\sigma}$  ( $b_{i,\sigma}^\dagger$ ) annihilates (creates) electrons at the site  $\mathbf{R}_i$  with spin  $\sigma$  ( $\sigma = \uparrow, \downarrow$ ) on sublattice B.  $t$  and  $t'$  are the nearest neighbor and next-nearest neighbor hopping energies respectively, and  $\mu$  is the chemical potential. The presence of  $t'$  introduces an asymmetry between the valance and conduction bands, thus violating particle-hole symmetry. Specific values for  $t$  and  $t'$  have been estimated<sup>25</sup> by comparing a tight-binding description to first-principle calculations. Following their estimates, we take  $t = 2.7\text{eV}$ . To learn more on the effect of  $t'$  in graphene, cases with different values of  $t'$  will be studied, and a typical  $t' = 0.27\text{eV}$  will be paid more attention<sup>23</sup> in the following.

In the sublattice system, there are two coupled sublattices, and the energy spectrum has two branches. In this case, the one-particle Green's functions are matrices

$$g(i-j, \tau) = \begin{pmatrix} g_{aa}(i-j, \tau) & g_{ab}(i-j, \tau) \\ g_{ba}(i-j, \tau) & g_{bb}(i-j, \tau) \end{pmatrix}, \quad (2)$$

where the longitudinal and transverse parts are defined as

$$g_{mn}(i-j, \tau) = -\langle T_\tau m_i(\tau) n_j^\dagger(0) \rangle, m, n = a, b; \quad (3)$$

with  $\tau$  is the imaginary time, and  $T_\tau$  is the  $\tau$  order operator. Then the Green's functions are obtained as

$$g_{aa}(k, \omega) = \frac{1}{2} \sum_{\nu=1,2} \frac{1}{\omega - \xi_k^{(\nu)}} = g_{bb}(k, \omega), \\ g_{ab}(k, \omega) = \frac{1}{2} \frac{\phi_k}{|\phi_k|} \sum_{\nu=1,2} (-1)^\nu \frac{1}{\omega - \xi_k^{(\nu)}} = g_{ba}^*(k, \omega) \quad (4)$$

respectively, where

$$\xi_k^{(\nu)} = t' \gamma_k + \mu + 2t |\phi_k| (-1)^{\nu+1}, \\ \phi_k = [e^{ik_x} + e^{i(\frac{1}{2}k_x + \frac{\sqrt{3}}{2}k_y)} + e^{i(\frac{1}{2}k_x - \frac{\sqrt{3}}{2}k_y)}], \\ \gamma_k = 2[\cos \sqrt{3}k_x + 2 \cos \frac{3}{2}k_x \cos(\frac{\sqrt{3}}{2}k_y)]. \quad (5)$$

From these, the DOS follows as

$$\rho(\omega) = -\frac{2}{\pi} \frac{1}{N} \sum_k \text{Im} g_{aa}(k, \omega + i\Gamma), \quad (6)$$

with  $\Gamma \rightarrow 0^+$ . For  $t' = 0$  an analytical expression for the DOS per unit cell can be derived<sup>18</sup>:

$$\rho_0(\omega) = \frac{1}{N} \sum_{k\nu} \delta[\omega - (-1)^\nu t \sqrt{3 + \gamma_k}] \\ = \frac{2}{\pi^2} \frac{|\omega|}{t^2} \frac{1}{\sqrt{Z_0}} \mathbf{K}[Z(\omega)], \quad (7)$$

where  $Z(\omega) = \sqrt{\frac{Z_1}{Z_0}}$  with

$$Z_0 = \frac{1}{4}(1 + \frac{|\omega|}{t})^3(3 - \frac{|\omega|}{t}), Z_1 = 4\frac{|\omega|}{t}, |\omega| \leq t \\ Z_1 = \frac{1}{4}(1 + \frac{|\omega|}{t})^3(3 - \frac{|\omega|}{t}), Z_0 = 4\frac{|\omega|}{t}, t < |\omega| < 3t, \quad (8)$$

and  $\mathbf{K}(x)$  is the complete elliptic integral of the first kind. With a finite  $t'$ , the DOS is evaluated by inserting unity in the form of an integral over the Dirac delta function as

$$\rho(\omega) = \frac{1}{N} \sum_{k\nu} \delta[1 - \xi(k)^{(\nu)}] \\ = \frac{1}{N} \sum_{k,\nu} \delta(1 - \xi(k)^{(\nu)}) \\ \times \frac{1}{2} \sum_{\lambda=1,2} \int_{-\infty}^{\infty} d\epsilon \delta[\epsilon - (-1)^\lambda t \sqrt{3 + \gamma_k}]. \quad (9)$$

Then, by interchanging the integration with  $k$  summation, we obtain

$$\rho(\omega) = \frac{1}{2N} \sum_{k\nu\lambda} \int_{-\infty}^{\infty} d\epsilon \delta[\omega - t'(g_k^2 - 3) - (-1)^\nu t g_k] \delta[\epsilon - (-1)^\lambda t g_k] \quad (10)$$

with  $g_k = \sqrt{3 + \gamma_k}$ . The second delta function enables us to replace  $g_k$  by  $\epsilon/t(-1)^\lambda$ , yielding to

$$\rho(\omega) = \sum_{\nu} \int_{-\infty}^{\infty} d\epsilon \delta[\omega - t' \frac{\epsilon^2}{t^2} + 3t' - (-1)^\nu \epsilon] \\ \times \frac{1}{2N} \sum_{k\lambda} \delta[\epsilon - (-1)^\lambda t g_k] \\ = \sum_{\nu} \int_{-\infty}^{\infty} \frac{d\epsilon}{2} \delta[\omega - t' \frac{\epsilon^2}{t^2} + 3t' - (-1)^\nu \epsilon] \rho_0(\epsilon), \quad (11)$$

where  $\rho_0(\epsilon)$  is the DOS with  $t' = 0$ , and then

$$\rho(\omega) = \frac{1}{\sqrt{1 + 4\frac{t'}{t^2}(\omega + 3t')}} \frac{2}{\pi^2} \sum_{\nu} \frac{|\tilde{\omega}_{\nu}|}{t^2} \frac{1}{\sqrt{Z_0}} \mathbf{K}[Z(\tilde{\omega}_{\nu})],$$

$$\tilde{\omega}_{\nu} = \frac{t^2}{2t'} [1 + (-1)^{\nu} \sqrt{1 + 4\frac{t'}{t^2}(\omega + 3t')}] \quad (12)$$

Now let us turn to evaluate the NMR relaxation rate and the static spin susceptibility. In general,  $1/T_1$  measures the local dynamics of the spins, and it is related to the transverse spin susceptibility  $\chi_{\perp}(i\omega_n)$ , which reads as<sup>26</sup>

$$\chi_{\perp}(i\omega_n) = - \int_0^{\beta} d\tau e^{i\omega_n \tau} \langle T_{\tau} S_i^{\dagger}(\tau) S_i^{-}(0) \rangle, \quad (13)$$

and after a straightforward calculation, we obtain

$$\langle T_{\tau} S_i^{\dagger}(\tau) S_i^{-}(0) \rangle = \sum_{m,n} g_{mn}(0, \tau) g_{mn}(0, -\tau). \quad (14)$$

With the help of spectral representation, we define

$$A(k, \omega) = -2\text{Im} \sum_{m,n} g_{mn}(k, \omega), \quad (15)$$

which has a relationship with the DOS

$$\frac{1}{N} \sum_k A(k, \omega) = 2\pi \rho(\omega). \quad (16)$$

In this representation, we can obtain the NMR relaxation rate finally

$$\begin{aligned} \frac{1}{T_1 T} &= \lim_{\omega \rightarrow 0} \frac{k_B}{g^2 \mu_B^2 \hbar^2} \sum_k F^2(k) \frac{\text{Im} \chi_{\perp}(k, \omega)}{\omega} \\ &= \pi F^2 \int_{-\infty}^{\infty} \rho^2(\omega') \frac{\beta}{4} \frac{d\omega'}{\cosh^2(\beta \frac{\omega' - \mu}{2})}, \end{aligned} \quad (17)$$

in which  $\mu_B$  is the Bohr magneton,  $g$  is the electron  $g$  factor,  $\hbar$  is the Planck constant, and  $\beta = 1/k_B T$ , where  $k_B$  is the Boltzman constant. The  $F(k)$  are hyperfine form factors, which do not vary much with  $k$  in general. So we write all these form factors as  $F$ , which is independent of temperature. In the similar way, the static spin susceptibility can be derived as

$$\begin{aligned} \chi &= \lim_{q \rightarrow 0} \lim_{\omega \rightarrow 0} \chi(q, \omega) \\ &= g^2 \mu_B^2 \int_{-\infty}^{\infty} \rho(\omega') \frac{\beta}{4} \frac{d\omega'}{\cosh^2(\beta \frac{\omega' - \mu}{2})}, \end{aligned} \quad (18)$$

and  $\chi(q, \omega)$  comes from

$$\chi(i - j, \tau) = - \int_0^{\beta} d\tau e^{i\omega_n \tau} \langle T_{\tau} S_i^z(\tau) S_j^z(0) \rangle. \quad (19)$$

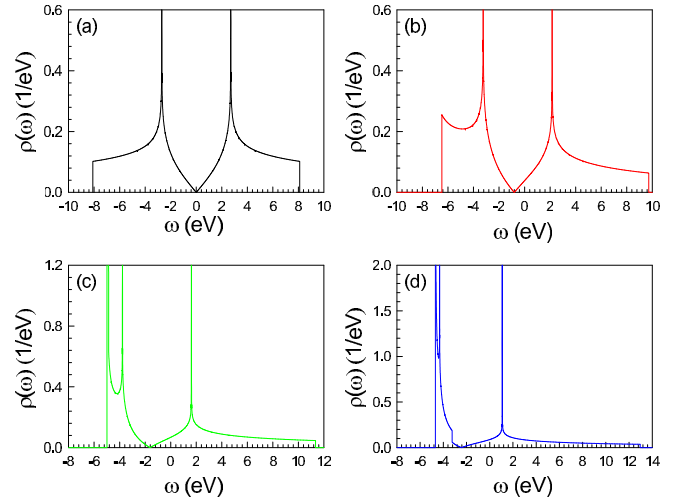


FIG. 1: DOS for different values of the next nearest neighbor hopping  $t'$ : (a)  $t' = 0$ ; (b)  $t' = 0.27$  eV; (c)  $t' = 0.54$  eV; (d)  $t' = 0.81$  eV with  $t = 2.7$  eV.

### III. RESULTS AND DISCUSSIONS

NMR is a powerful method to characterize correlated states of materials as it is sensitive to the DOS near the Fermi edge. So we study the DOS firstly, and our results for different values of the next neighbor hoping  $t'$  have been shown in Fig.1. Focusing on the particle-hole symmetric case, in Fig.1 (a), it is clear that, besides the linear vanishing of the DOS at the Fermi level, there are marked van Hove singularities at the hopping energy,  $\omega = \pm t$ . With a finite  $t'$ , as shown in Fig.1 (b), (c) and (d), these van Hove singularities shall appear at  $\tilde{\omega}_{\nu} = \pm t$ , which is derived from Eq. 12, and we will show that  $t'$  plays an important role in graphene as it breaks the particle-hole symmetry.

For both  $t' = 0$  and  $t' \neq 0$  cases, the DOS in graphene is markedly different from that in normal metals<sup>24</sup> as its low energy excitations are two-dimensional massless Dirac fermions<sup>3,4</sup>, and the presence of  $t'$  shifts in energy the position of the Dirac point and breaks particle-hole symmetry. Our further results shall indicate that these kinds of important features of the DOS are at the origin of interesting properties of the NMR relaxation rate and the static spin susceptibility in graphene, as well as many transport anomalies in this material<sup>18</sup>.

Having been familiar with the main features of the DOS in graphene, we now turn to the evaluation of the NMR relaxation rate and the static spin susceptibility. In Fig.2 (a) and (b), the NMR relaxation rate and the static spin susceptibility as a function of  $t'$  for  $t = 2.7$  eV,  $T = 10$  K at  $\mu = 0$  are plotted respectively. As shown by the dark line in Fig.2 (a), the NMR relaxation rate follows a  $t'^2$  power law at  $\mu = 0$ , while the static spin susceptibility is linearly dependent on  $t'$  as indicated by the dark line in Fig.2(b). One of the most important properties of the NMR relaxation rate is its temperature dependent be-

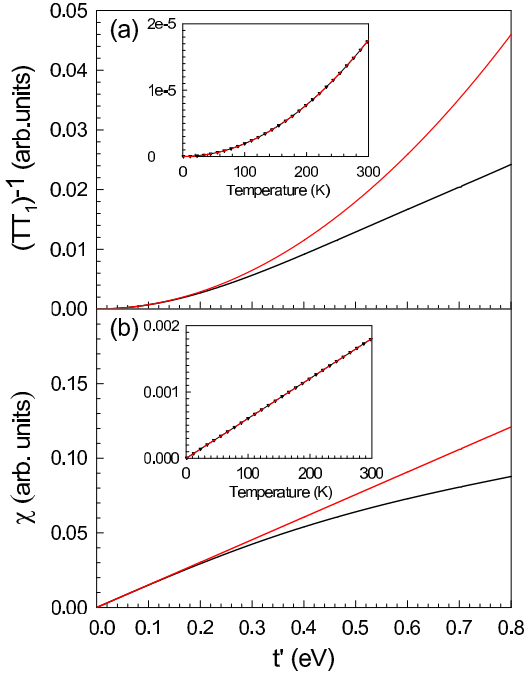


FIG. 2: (a) The NMR relaxation rate and (b) the static spin susceptibility as function of  $t'$  for  $t=2.7$  eV,  $T=10$ K at  $\mu=0$ . Dark lines indicate the exact numerical result and red lines indicate data computed from Eq. 21 or Eq. 22. Inset: (a) The NMR relaxation rate and (b) the static spin susceptibility as function of temperature  $T$  for  $t=2.7$  eV,  $t'=0$ , and  $\mu=0$ . Dark lines with triangle indicate the exact numerical result and dash red lines indicate data computed from Eq. 21 or Eq. 22.

havior. In the inset of Fig.2(a) and (b), we have plotted the temperature dependence of the NMR relaxation rate and the static spin susceptibility respectively at  $t=2.7$  eV,  $t'=0$  and  $\mu=0$ . As indicated by the dark lines with triangle, the NMR relaxation rate follows a  $T^2$  power law, and the static spin susceptibility is linearly dependent on temperature  $T$ .

With a finite chemical potential  $\mu$  and  $t'$ , the approximate behavior of the NMR relaxation rate and the static spin susceptibility may be expressed analytically at low temperatures. From Eq.17, we see that only low energy part shall contribute to the NMR relaxation rate due to the properties of Fermi function at low temperatures. When  $|\tilde{\omega}_\nu| \ll t$ , as well as  $t' \ll t$ , the DOS may be expressed as

$$\rho(\omega) \simeq \frac{2\sqrt{3}}{3\pi} \frac{|\omega + 3t'|}{t^2} \quad (20)$$

approximately, and finally

$$\frac{1}{T_1 T} \simeq F^2 \frac{4}{3\pi} \frac{1}{t^4} [(\mu + 3t')^2 + \frac{\pi^2}{3} k_B^2 T^2]. \quad (21)$$

In this similar way, the static spin susceptibility may be

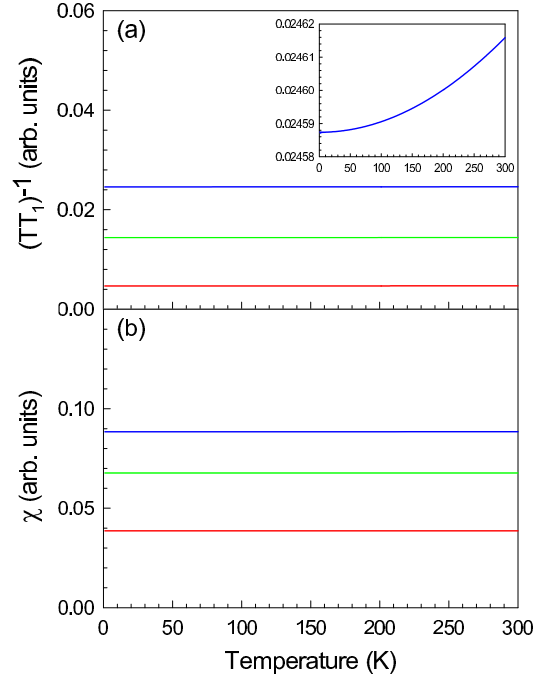


FIG. 3: (Color online ) (a) The NMR relaxation rate and (b) the static spin susceptibility as function of temperature for  $t=2.7$  eV with  $t'=0.27$  eV (red line),  $t'=0.54$  eV (green line),  $t'=0.81$  eV (blue line) at  $\mu=0$ . Inset: Enlarge scale for  $t'=0.81$  eV.

approximated by

$$\chi \simeq g^2 \mu_B^2 \frac{2\sqrt{3}}{3\pi} \frac{1}{t^2} \{(\mu + 3t') + 2k_B T \ln[1 + e^{-\beta(\mu + 3t')}] \} \quad (22)$$

The data computed within Eq.21 and Eq.22 have also been shown in Fig.2, which are indicated by red lines, and each of them is very near to the exact result especially when  $t' < 0.2$  eV.

The calculated temperature dependence of the NMR relaxation rate and the static spin susceptibility for different values of  $t'$  at  $\mu = 0$  are shown in Fig.3 (a) and (b) respectively. At first glance, it seems that the NMR relaxation rate and the static spin susceptibility are almost independent of temperature for a fixed  $t'$ . In the inset of Fig.3(b), we enlarged the scale for the case of  $t'=0.81$  eV, and the NMR relaxation rate increases as temperature increases, following a  $T^2$  power law. However, the enhancement with temperature is rather small comparing with the whole trend.

This unusual phenomenon is a direct results of the low energy excitations of graphene, which behave as massless Dirac fermions. In low energy regime, the DOS in graphene is linear around the particle-hole symmetric filling, and vanishes at the Dirac point, while the presence of  $t'$  shifts in energy the position of the Dirac point. Mathematically it is clearly seen through Eq.20. Hence, with a finite chemical potential  $\mu$  and  $t'$ , we can describe our result within Eq.21 and Eq.22 at low temperatures rather well. In the particle-hole symmetric case, namely,  $t'=0$ ,

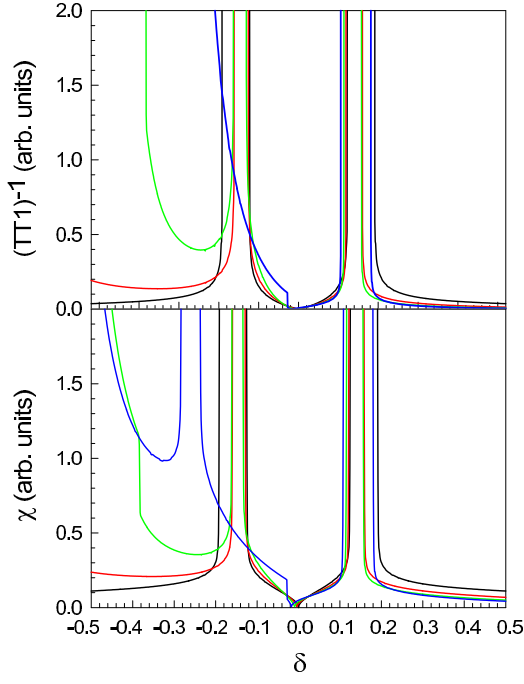


FIG. 4: (Color online) (a) The NMR relaxation rate and (b) the static spin susceptibility as function of the excess charge for  $t=2.7$  eV with  $t'=0$  (dark line),  $t'=0.27$  eV (red line),  $t'=0.54$  eV (green line) and  $t'=0.81$  eV (blue line) at  $T=10$ K.

the NMR relaxation rate follows a  $T^2$  power law. However, the  $T^2$  term in the NMR relaxation rate is negligible with respect to  $(\mu + 3t')$  for realistic values of  $\mu$  and  $t'$ . On the static spin susceptibility, it is linearly dependent on  $T$  at half filling when  $t' = 0$ , while with a finite  $\mu$  and  $t'$ , it should be dominated by  $(\mu + 3t')$  terms in low energy regime, which may be described by Eq.22 very well. Our results also show that  $t'$  plays an important role in graphene since it breaks the particle-hole symmetry and is responsible for various effects observed experimentally.

Arguably, one of the most interesting and promising properties from the technological point of view is the ability to tune the carrier density in graphene through a gate voltage<sup>1</sup>. Now let's turn to study the case with a finite excess charge  $\delta$ , and the chemical potential  $\mu$  is determined by

$$\int_{-\infty}^{\infty} \rho(\omega) \left[ \frac{1}{e^{\beta(\omega-\mu)} + 1} - \frac{1}{2} \right] d\omega = \delta. \quad (23)$$

With the help of the gate voltage, one can control the density and type ( $n$  or  $p$ ) of carriers varying their chemical potential<sup>4</sup>. The calculated  $\delta$  dependence of the NMR relaxation rate and the static spin susceptibility for different values of  $t'$  have been shown in Fig.4 (a) and (b) respectively. The NMR relaxation rate and the static spin susceptibility are linearly dependent on  $|\delta|$  when  $|\delta| < 0.1$  except  $t'=0.81$  eV. While  $\delta$  is high enough, it is interesting to find that there are several prominent peaks. In the particle-hole symmetric case, peaks appear around the

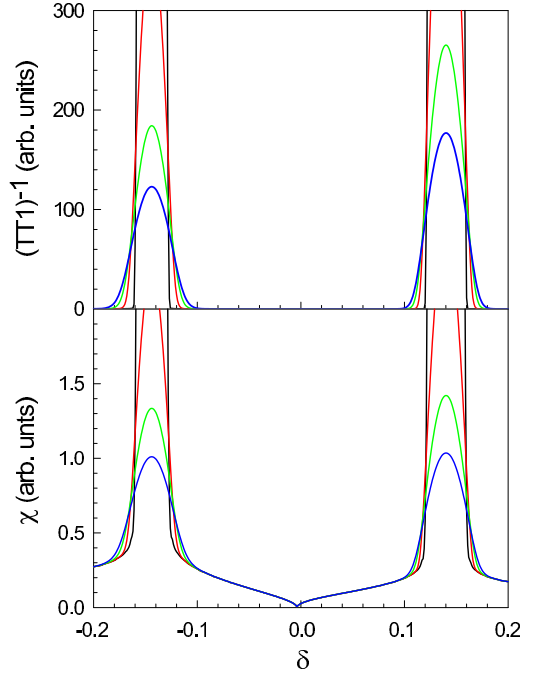


FIG. 5: (Color online) (a) The NMR relaxation rate and (b) the static spin susceptibility as function of  $\delta$  for  $t=2.7$  eV,  $t'=0.27$  eV at different temperatures:  $T=10$ K (dark line),  $T=100$ K (red line),  $T=200$ K (green line) and  $T=300$ K (blue line).

center at  $\delta=\pm 0.157$ . With a finite  $t'$ , these peaks shall appear around the center at  $\delta=0.140, -0.144$  for  $t'=0.27$  eV,  $\delta=0.136, -0.147$  for  $t'=0.54$  eV, and  $\delta=0.144, -0.260$  for  $t'=0.81$  eV.

These intriguing phenomenon may be predicted from the behavior of the DOS in graphene directly. When the chemical potential is located at the marked van Hove singularities, where the DOS peaks dramatically, hence peaks shall appear in the NMR relaxation rate and the static spin susceptibility<sup>20</sup>. To learn more on these peaks, the calculated  $\delta$  dependence of the NMR relaxation rate and the static spin susceptibility with  $t=2.7$  eV,  $t'=0.27$  eV at different temperatures are plotted in Fig.5 (a) and (b) respectively. These peaks in the NMR relaxation rate and the static spin susceptibility decrease as the temperature increases, however, these peaks are even pronounced at 300 K, and therefore, there peaks should produce a distinct effect on temperature dependence of the NMR relaxation rate and the static spin susceptibility.

In Fig.6 (a) and (b), we plot the NMR relaxation rate and the static spin susceptibility as function of temperature at different  $\delta$  for  $t=2.7$  eV and  $t'=0.27$  eV. Around  $\delta=0.12$ , we can immediately separate the data into two temperature regimes by a crossover: the high temperature regime and the low temperature regime. The NMR relaxation rate and the static spin susceptibility increase dramatically as temperature increases in the low temperature regime, and after the crossover, both of them



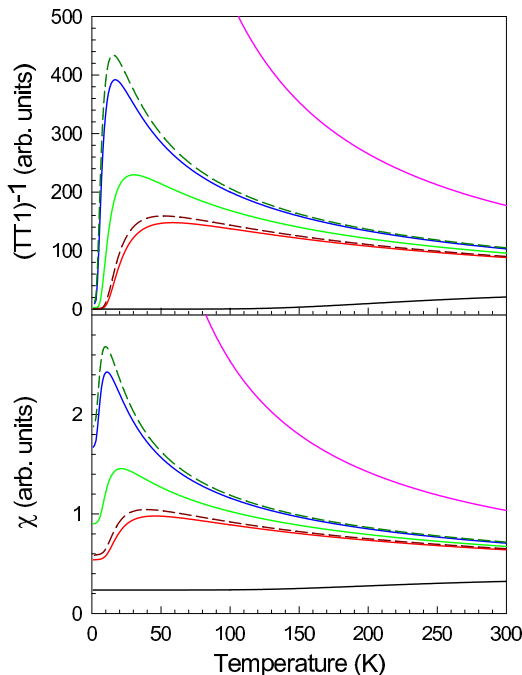


FIG. 6: (Color online) (a) The NMR relaxation rate and (b) the static spin susceptibility as function of temperature  $T$  for  $\delta=0.11$  (dark line),  $\delta=0.12$  (red line),  $\delta=0.121$  (green line), and  $\delta=0.122$  (blue line),  $\delta=0.14$  (pink line),  $\delta=0.158$  (dash-dark-green line), and  $\delta=0.16$  (dash-dark-red line) at  $t=2.7$  eV and  $t'=0.27$  eV.

decrease as temperature increases, and the position of temperature dependent crossover is sensitive to  $\delta$ .

For a fixed  $\delta$ , the chemical potential varies slightly as temperatures varies, so when the chemical potential associated with the temperature is located at the van Hove singularities, where the DOS peaks dramatically, there shall be peaks in both of the NMR relaxation rate and the static spin susceptibility, which may divide the temperature dependence of the NMR relaxation rate and the static spin susceptibility into two temperature regimes. The temperature at the crossover decreases as  $\delta$  increases when  $\delta < 0.140$ . As  $\delta$  tends toward 0.140, the NMR relaxation rate and the static spin susceptibility shall decrease as temperature increases almost in the whole temperature regime for current parameters, for instance, pink lines in Fig.6 (a) and (b); and afterward, the temperature at the crossover increases as  $\delta$  increases when  $\delta > 0.140$  (dash lines in Fig. 6 (a) and (b) are respect to this illumination ). We only analyze the case when  $\delta > 0$  at  $t' = 0.27$  eV; because, for other values of  $t'$  or

when  $\delta < 0$ , the essential nature of peak's appearing is the same.

#### IV. SUMMARY

In summary, we have analyzed the NMR relaxation rate and the static spin susceptibility in graphene, which show a behavior that is not that of a normal metal. In low energy regime, the DOS in graphene is linear around the particle-hole symmetric filling, and vanishes at the Dirac point, while the presence of  $t'$  shifts in energy the position of the Dirac point. Hence, the NMR relaxation rate follows a power law as  $T^2$  on the particle-hole symmetric side at half filling, while away from half filling and with a finite  $t'$ , the  $(\mu + 3t')^2$  terms dominate at low excess charge. The static spin susceptibility is linearly dependent on  $T$  at half filling when  $t' = 0$ , while with a finite  $\mu$  and  $t'$ , it should be dominated by  $(\mu + 3t')$  terms in low energy regime. The next-nearest neighbor  $t'$  plays an important role in graphene as it breaks the particle-hole symmetry and is responsible for various effects observed experimentally. These unusual phenomena are direct results of the low energy excitations of graphene.

The NMR relaxation rate and the static spin susceptibility are linearly dependent on the excess charge  $|\delta|$  when  $|\delta|$  is small, while at high  $\delta$ , there is a pronounced crossover which divides the temperature dependence of the NMR relaxation rate and the static spin susceptibility into two temperature regimes: the NMR relaxation rate and the static spin susceptibility increase dramatically as temperature increases in the low temperature regime, and after the crossover, both decrease as temperature increases at high temperatures. This crossover is due to the well-known logarithmic Van Hove singularity in the DOS, and its position dependence of temperature is sensitive to  $\delta$ . These properties show that graphene is a new class of materials with an unusual metallic state. Since the electronic density is easily controlled by a gate voltage, these phenomena can certainly be tested experimentally.

#### Acknowledgments

We acknowledge useful discussions with P. Thalmeier and K. Ziegler. This work was supported by the Hungarian Scientific Research Fund under grant number OTKA K72613.

<sup>1</sup> K. S. Novoselov, A. K. Geim, S. V. Morozov, D. Jiang, Y. Zhang, S. V. Dubonos, I. V. Grigorieva, and A. A. Firsov, *Science* **306**, 666 (2004).

<sup>2</sup> P. R. Wallace, *Phys. Rev.* **71**, 622 (1947).

<sup>3</sup> G. W. Semenoff, *Phys. Rev. Lett.* **53**, 2449 (1984).

<sup>4</sup> A. K. Geim and K. S. Novoselov, *Nature Materials* **6**, 183 (2007).

<sup>5</sup> K. S. Novoselov, A. K. Geim, S. V. Morozov, D. Jiang, M.

- I. Katsnelson, I. V. Grigorieva, S. V. Dubonos, and A. A. Firsov, *Nature* **438**, 197 (2005).
- <sup>6</sup> Y. B. Zhang, Y. W. Tan, H. L. Stormer, and P. Kim, *Nature* **438**, 201 (2005).
  - <sup>7</sup> K. S. Novoselov, Z. Jiang, Y. Zhang, S. V. Morozov, H. L. Stormer, U. Zeitler, J. C. Mann, G. S. Boebinger, P. Kim, and A. K. Germ, *Science* **315**, 1379 (2007).
  - <sup>8</sup> K. Yang, *Solid State Commun.* **143**, 27 (2007).
  - <sup>9</sup> K. Ziegler, *Phys. Rev. Lett.* **97**, 266802 (2006).
  - <sup>10</sup> K. Nomura and A. H. MacDonald, *Phys. Rev. Lett.* **98**, 076602 (2007).
  - <sup>11</sup> H. B. Heersche, P. Jarillo-Herrero, J. B. Oostinga, L. M. K. Vandersypen, and A. F. Morpurgo, *Nature* **446**, 56 (2007).
  - <sup>12</sup> M. A. H. Vozmediano, M. P. López-Sancho, T. Stauber and F. Guinea, *Phys. Rev. B* **72**, 155121 (2005).
  - <sup>13</sup> Z. Jiang, E. A. Henriksen, L. C. Tung, Y.-J. Wang, M. E. Schwartz, M. Y. Han, P. Kim, and H. L. Stormer, *Phys. Rev. Lett.* **98**, 197403 (2007); A. B. Kuzmenko, E. van Heumen, F. Carbone, and D. van der Marel, arXiv:0712.0835.
  - <sup>14</sup> B. Uchoa and A. H. Castro Neto, *Phys. Rev. Lett.* **98**, 146801 (2007); A. Bostwick, T. Ohta, T. Seyller, K. Horn, and E. Rotenberg, *Nature Physics* **3**, 36 (2007).
  - <sup>15</sup> C. L. Kane and E. J. Mele, *Phys. Rev. Lett.* **95**, 226801 (2005).
  - <sup>16</sup> S. Cho, Y.-F. Chen, and M. S. Fuhrer, *Appl. Phys. Lett.* **91**, 123105 (2007).
  - <sup>17</sup> Y. G. Yao, F. Ye, X.-L. Qi, S.-C. Zhang, and Z. Fang, *Phys. Rev. B* **75**, 041401(R) (2007).
  - <sup>18</sup> A. H. Castro Neto, F. Guinea, N. M. R. Peres, K. S. Novoselov, and A. K. Geim, arXiv:0709.1163 (2007).
  - <sup>19</sup> C. P. Slichter, *Principles of Magnetic Resonance* (Springer-Verlag, New York, 1989), 3rd ed.
  - <sup>20</sup> P. Bénard, L. Chen, and A.-M. S. Tremblay, *Phys. Rev. B* **47**, 15217 (1993).
  - <sup>21</sup> P. M. Singer, P. Wzietek, H. Alloul, F. Simon, and H. Kuzmany, *Phys. Rev. Lett.* **95**, 236403 (2005).
  - <sup>22</sup> B. Dóra, M. Gulácsi, F. Simon, and H. Kuzmany, *Phys. Rev. Lett.* **99**, 166402 (2007).
  - <sup>23</sup> N. M. R. Peres, F. Guinea, and A. H. Castro Neto, *Phys. Rev. B* **73**, 125411 (2006).
  - <sup>24</sup> C. Benal and S. A. Kivelson, *Phys. Rev. B* **72**, 125432 (2005).
  - <sup>25</sup> S. Reich, J. Maultzsch, C. Thomsen, and P. Ordejón, *Phys. Rev. B* **66**, 035412 (2002).
  - <sup>26</sup> See, for example, S. Doniach and E.H. Sondheimer, *Green's Functions for Solid State Physicists* (W.A. Benjamin, Reading, Massachusetts, 1998).